

Sensor and Simulation Notes

Note 237

March 1978

CLEARED
FOR PUBLIC RELEASE

PL/PA 5-12-87

An Electric-Field-Penetration
Simulator for Apertures

F.C. Yang

Lennart Marin

Dikewood Corporation, Westwood Research Branch
Los Angeles, California 90024

Abstract

A technique for simulating the electric-field penetration through apertures is considered. The simulator consists of an electrically charged disk located above an aperture in a ground plane. The following quantities are calculated: (1) capacitance between the disk and the ground plane, (2) dipole moment of aperture both in the presence and absence of the aperture, (3) simulator's effective height, equivalent area, and equivalent volume.

ACKNOWLEDGEMENT

The authors wish to thank Drs. C.E. Baum and J.P. Castillo of the Air Force Weapons Laboratory and Dr. K.S.H. Lee of the Dikewood Corporation, Westwood Research Branch for their many helpful suggestions and technical discussions during the course of this work. Mr. Terry Brown of Dikewood's Albuquerque office worked on the numerical calculations of this report.

PL 96-1242

Sensor and Simulation Notes

Note 237

March 1978

An Electric-Field-Penetration
Simulator for Apertures

F.C. Yang

Lennart Marin

Dikewood Corporation, Westwood Research Branch
Los Angeles, California 90024

Abstract

A technique for simulating the electric-field penetration through apertures is considered. The simulator consists of an electrically charged disk located above an aperture in a ground plane. The following quantities are calculated: (1) capacitance between the disk and the ground plane, (2) dipole moment of aperture both in the presence and absence of the aperture, (3) simulator's effective height, equivalent area, and equivalent volume.

ACKNOWLEDGEMENT

The authors wish to thank Drs. C.E. Baum and J.P. Castillo of the Air Force Weapons Laboratory and Dr. K.S.H. Lee of the Dikewood Corporation, Westwood Research Branch for their many helpful suggestions and technical discussions during the course of this work. Mr. Terry Brown of Dikewood's Albuquerque office worked on the numerical calculations of this report.

apertures, electric fields, dipoles, electromagnetic pulse simulation

CONTENTS

<u>Section</u>	<u>Page</u>
I INTRODUCTION	5
II FORMULATION OF THE PROBLEM	9
1. An Integral Expression for the Electrostatic Potential	9
2. Formulation of an Integral Equation	13
III CHARACTERISTIC QUANTITIES OF SIMULATOR	18
1. Capacitance Between Disk and Perforated Ground Plane	18
2. Dipole Moment of Aperture	19
3. Simulator's Effective Height	20
4. Simulator's Equivalent Area and Volume	23
IV SOME LIMITING CASES	27
1. The Case $h \gg a$, $h \gg b$	27
2. The Case $b \ll a$	28
3. The Case $a = 0$	29
4. The Case $h = 0$, $a > b$	29
V NUMERICAL CALCULATIONS	30
1. Approximation of (17) by a Matrix Equation	30
2. Accuracy of Numerical Solution	22
3. Numerical Results for C , p , h_{eff} , A_{eq} and V_{eq}	33
REFERENCES	41

ILLUSTRATIONS

<u>Figure</u>		<u>Page</u>
1	Common Apertures in Aircraft.	6
2	An Aperture-Electric-Field-Penetration Simulator.	7
3	An Electric-Field Simulator Consisting of a Circular Disk Located Above a Circular Aperture in a Ground Plane.	10
4	The Receiving Problem (a) and the Capacitance Problem (b) Used in the Lorentz Reciprocity Theorem.	21
5	The Simulator Problem Defining the Equivalent Area.	24
6	The Low Frequency Thévenin and Norton Equivalent Circuits of the Simulator.	25
7	Capacitance, Equivalent Area, and Equivalent Volume of a Circular Disk Above a Ground Plane. The Broken Curves Correspond to the Asymptotic Results of Equation (38).	34
8	Variation of Simulator Capacitance with Position of Disk and Size of Aperture. The Values are Normalized with Respect to the Capacitance in the Absence of the Aperture. The Broken Curves Correspond to the Asymptotic Results of Equation (38).	35
9	Variation of the Aperture Dipole Moment with Position and Size of Simulator Disk.	36
	(a) The Values are Normalized with Respect to the Dipole Moment of the Aperture when Subject to a Uniform, Normal Electric Field of Strength V_0/h .	
	(b) The Values are Normalized with Respect to the Limiting Value of the Dipole Moment as $h/a \ll 1$ and $b/a \gg 1$.	
	The Broken Curves Correspond to the Asymptotic Results of Equation (41)	

ILLUSTRATIONS (Continued)

<u>Figure</u>		<u>Page</u>
10	Variation of Simulator Effective Height with Position of Disk and Size of Aperture. The Broken Curves Correspond to the Asymptotic Results of Equation (41).	37
11	Variation of Simulator Equivalent Area with Position of Disk and Size of Aperture. The Values are Normalized with Respect to the Equivalent Area in the Absence of the Aperture. The Broken Curves Correspond to the Asymptotic Results of Equation (41).	38
12	Variation of Simulator Equivalent Volume with Position of Disk and Size of Aperture. The Values are Normalized with Respect to the Equivalent Volume in the Absence of the Aperture. The Broken Curves Correspond to the Asymptotic Results of Equation (41).	39

TABLES

<u>Table</u>		
1	COMPARISONS OF THE CAPACITANCE AND EQUIVALENT AREA BETWEEN THE PRESENT RESULTS AND THOSE OF LATHAM AND LEE GIVEN IN REFERENCE 5.	33

SECTION I

INTRODUCTION

A fullfledged test of the electromagnetic pulse (EMP) hardness of military systems such as the E-4, E-3A, EC-135 or the Minuteman in a large EMP simulator is a very time consuming and costly procedure. These tests are, however, necessary to find all the ways through which electromagnetic energy can penetrate into the system. Once the various ports of entry (POE's) of electromagnetic (EM) energy have been found, means of eliminating them can be devised. Some of the devices used in eliminating the POE's (usually referred to as hardening fixes) may degrade during the life span of the system. This in turn implies that a presumably "EMP hard" system may not be as hard as initially intended. For reasons cited above, it is important to have simple, inexpensive ways (that can be used in the field) of testing the EMP hardness of a particular system.

One important type of POE on aircraft is an aperture. Apertures can be either hatched ones (occurring around various doors, figure 1a) or simple ones such as windows (figure 1b). The hatched apertures can be electromagnetically sealed by covering them with a conducting gasket (figure 1c). The EMP energy that penetrates through windows can be considerably diminished by placing a mesh of conducting wires over the window (figure 1d).

Most apertures on aircraft are electrically small implying that the electric and magnetic field penetrations can be separated and simulated independently. In this report we will limit ourselves to the simulation of electric-field penetration into an aperture. The magnetic-field penetration will be left to a future effort.

One way of simulating the electric-field penetration through an aperture is shown in figure 2, where a disk is placed above the aperture. Since we are considering a quasi-electrostatic situation, the time history of the simulated aperture field is proportional to the disk voltage $V(t)$. This time history should of course equal the time history of the charge density on the aircraft at the location of the aperture when it is covered (short circuited) and the aircraft is subject to an incident EMP. Thus, the

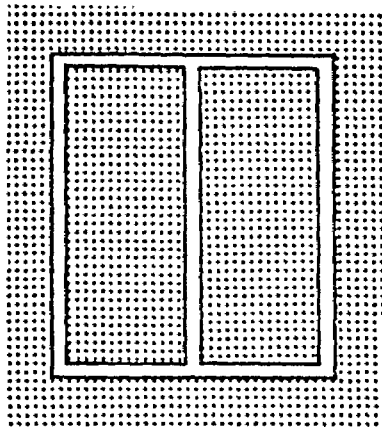


figure 1a, hatched aperture

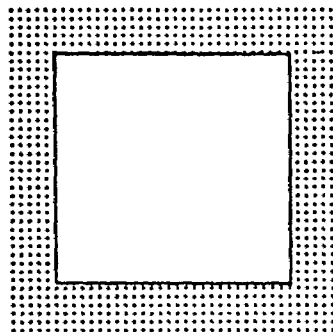


figure 1b, window

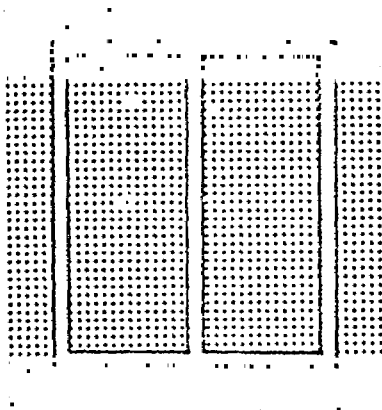


figure 1c, hatched aperture
with conducting gasket

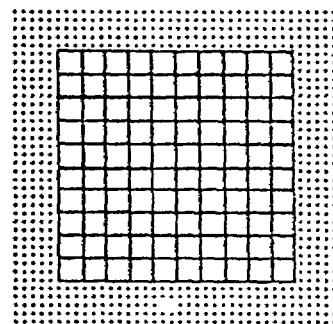


figure 1d, window with a
mesh of conducting wires

Figure 1. Common Apertures in Aircraft.

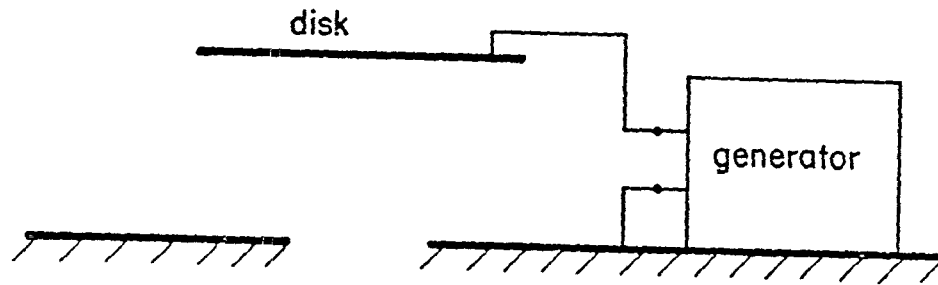
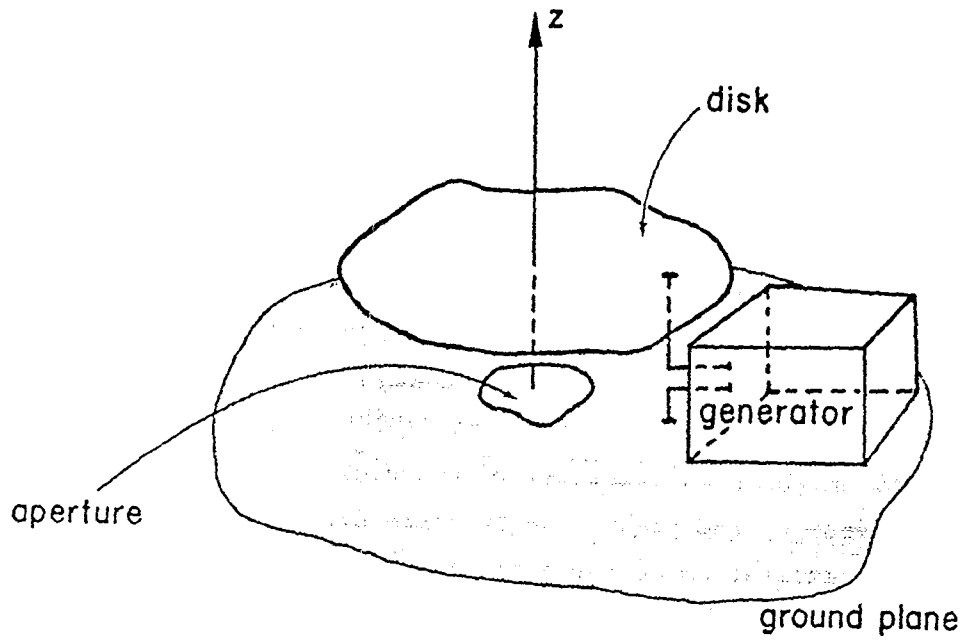


Figure 2. An Aperture-Electric-Field Penetration Simulator.

generator shown in figure 2 must be designed so that the voltage V has the required time history. To do that it is necessary to know the capacitance C between the simulator disk and the aircraft in the presence of the aperture. We will determine this capacitance in the present report for a particular simulator-aperture geometry.

The interaction between the disk (simulator) and the aperture (test object) implies that the simulated field distribution in the aperture is different from the actual EMP-induced one. As a measure of this interaction we use the normalized dipole moment (or polarizability) of the aperture. Consequently, we determine the polarizability of the aperture both in the presence and in the absence of the disk. The aperture dipole moment is also proportional to the excitation of the aperture (e.g. the field strength at the aperture's midpoint). The simulator's effective height, equivalent area, and equivalent volume are also considered.

To obtain a problem that is amenable to analysis we assume that the aperture is circular and that the simulator disk is also circular and coaxial with the aperture. This problem is reduced to the solution of a Fredholm integral equation of the second kind by using Whittaker's solution of Laplace's equation for rotationally symmetric objects. The integral equation is solved analytically in some limiting cases and numerically in the general case. The results of this report can be used for noncircular apertures and disks provided that the respective areas are equated.

It should be pointed out that the simulator discussed in this report is of the FINES type. The general aspects of the FINES-type simulator are discussed in references 1,2, and 10.

SECTION II

FORMULATION OF THE PROBLEM

Consider the problem of figure 3 where a circular disk is kept at the potential V_0 versus the perforated ground plane. The aperture in the ground plane is circular and coaxial with the disk. Based on Whittaker's solution of Laplace's equation (ref. 3) we will formulate in this section an integral equation for the problem at hand. The solution of this integral equation will yield all the desired information sought, i.e., the capacitance between the simulator disk and the ground plane as well as the simulator's effective height, equivalent area, and equivalent volume.

1. AN INTEGRAL EXPRESSION FOR THE ELECTROSTATIC POTENTIAL

From Whittaker's solution of the rotationally symmetric potential problem (refs. 3, 4 and 5), the off-axis potential $\phi(\rho, z)$ can be expressed in terms of the on-axis potential $\phi(0, z)$ in the following manner:

$$\phi(\rho, z) = \frac{1}{\pi} \int_0^\pi \phi(0, z + i\rho \cos \phi) d\phi \quad (1)$$

The on-axis potential is simply given by

$$\begin{aligned} \phi(0, z) &= \frac{1}{2\epsilon_0} \int_0^b \frac{\sigma_d(\rho') \rho' d\rho'}{\sqrt{\rho'^2 + (z-h)^2}} + \frac{1}{2\epsilon_0} \int_a^\infty \frac{\sigma_p(\rho') \rho' d\rho'}{\sqrt{\rho'^2 + z^2}} \\ &\equiv \phi_d(z) + \phi_p(z) \end{aligned} \quad (2)$$

where $\sigma_d(\rho')$ and $\sigma_p(\rho')$ are, respectively, the charge distribution on the disk and the ground plane. The expression (2) for $\phi_d(z)$ and $\phi_p(z)$ has been derived from Coulomb's law under the assumption that z is a real-valued variable. This expression can, however, be analytically continued

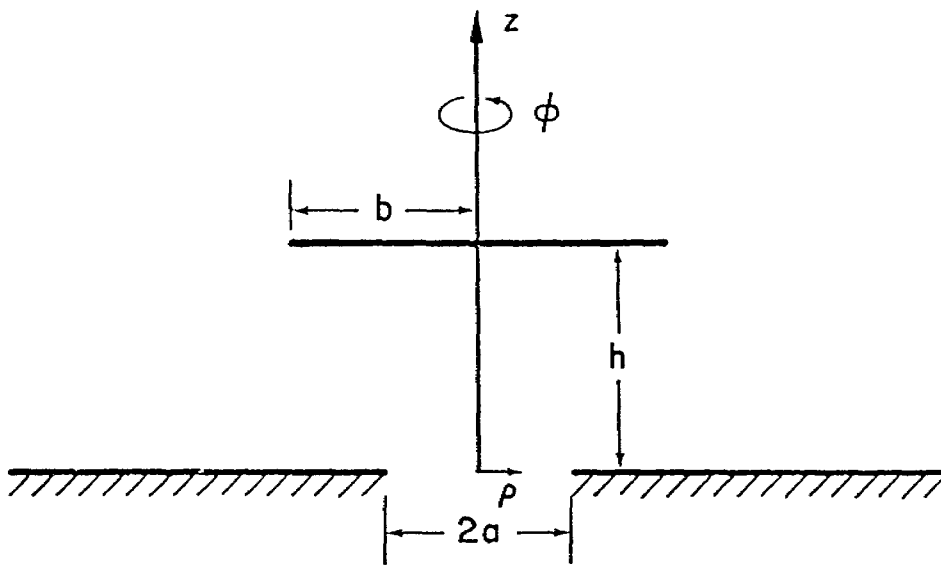
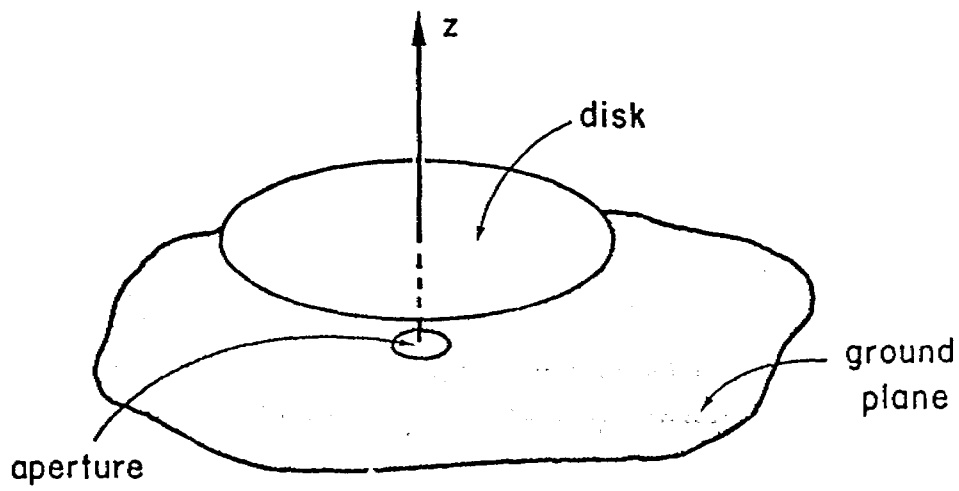


Figure 3. An Electric-Field Simulator Consisting of a Circular Disk Located Above a Circular Aperture in a Ground Plane.

to complex values of z . To determine the analytical properties of $\phi(0, z)$ in the complex z -plane we study $\phi_d(z)$ and $\phi_p(z)$ separately.

From the integral expression for $\phi_d(z)$, it is observed that this function has a branch cut between $z = h+ib$ and $z = h-ib$. Thus, $\phi_d(z)$ can be represented in the following manner by using the Cauchy theorem:

$$\begin{aligned}\phi_d(z) &= -\frac{V_o}{\pi i} \int_{h-ib}^{h+ib} \frac{f_d(\zeta)}{\zeta - z} d\zeta \\ &= -\frac{V_o}{\pi} \int_{-b}^b \frac{g_d(\eta)}{h+i\eta - z} d\eta\end{aligned}\tag{3}$$

Since $\phi_d(z)$ is a real-valued function for real values of z , $g_d(\eta)$ must satisfy the following condition:

$$g_d(-\eta) = g_d^*(\eta)\tag{4}$$

where the asterisk denotes complex conjugation.

The function $\phi_p(z)$ has two branch cuts: one between $-i\infty$ and $-ia$ and the other between $+ia$ and $+i\infty$. Thus, from Cauchy's integration theorem we have

$$\begin{aligned}\phi_p(z) &= -\frac{V_o}{\pi i} \int_{-i\infty}^{-ia} \frac{f_p^-(\zeta)}{\zeta - z} d\zeta - \frac{V_o}{\pi i} \int_{ia}^{i\infty} \frac{f_p^+(\zeta)}{\zeta - z} d\zeta \\ &= -\frac{V_o}{\pi} \int_{-\infty}^{-a} \frac{g_p^-(\eta)}{i\eta - z} d\eta - \frac{V_o}{\pi} \int_a^{\infty} \frac{g_p^+(\eta)}{i\eta - z} d\eta \\ &= -\frac{V_o}{\pi} \int_a^{\infty} \left[\frac{g_p^+(\eta)}{i\eta - z} - \frac{g_p^-(-\eta)}{i\eta + z} \right] d\eta\end{aligned}\tag{5}$$

To get some conditions from which to determine $g_p^\pm(\eta)$ we observe that $\phi_p(z)$ is the potential along the z -axis in figure 3 due to the charge density $\sigma_p(\rho)$ on the ground plane. The physics of the problem immediately implies that $d\phi_p/dz$ vanishes for $z=0$ and that $\phi_p(z)$ is real-valued for real values of z . For these two conditions to be satisfied it is required that

$$g_p^+(\eta) = -g_p^-(-\eta) = -i g_p(\eta) \quad (6)$$

To sum up, we have

$$\begin{aligned} \phi(z) &= \phi_d(z) + \phi_p(z) \\ &\equiv -\frac{V_0}{\pi} \int_0^b \left[\frac{g_d(\eta)}{h+i\eta-z} + \frac{g_d^*(\eta)}{h-i\eta-z} \right] d\eta \\ &\quad - \frac{V_0}{\pi i} \int_a^\infty \left[\frac{g_p(\eta)}{i\eta-z} + \frac{g_p(\eta)}{i\eta+z} \right] d\eta \end{aligned} \quad (7)$$

and

$$\begin{aligned} \phi(\rho, z) &= \frac{1}{\pi} \int_0^\pi \phi(z + i\rho \cos \phi) d\phi \\ &= -\frac{V_0}{\pi^2} \int_0^b \int_0^\pi \left[\frac{g_d(\eta)}{h+i\eta-z-i\rho \cos \phi} + \frac{g_d^*(\eta)}{h-i\eta-z-i\rho \cos \phi} \right] d\phi d\eta \\ &\quad - \frac{V_0}{\pi^2 i} \int_a^\infty g_p(\eta) \int_0^\pi \left[\frac{1}{i\eta-z-i\rho \cos \phi} - \frac{1}{-i\eta-z-i\rho \cos \phi} \right] d\phi d\eta \\ &= \frac{V_0}{\pi} \int_0^b \left[\frac{g_d(\eta)}{\sqrt{(h+i\eta-z)^2 + \rho^2}} + \frac{g_d^*(\eta)}{\sqrt{(h-i\eta-z)^2 + \rho^2}} \right] d\eta \end{aligned}$$

$$\begin{aligned}
& + \frac{V_0}{\pi i} \int_a^\infty g_p(\eta) \left[\frac{1}{\sqrt{(i\eta - z)^2 + \rho^2}} - \frac{1}{\sqrt{(-i\eta - z)^2 + \rho^2}} \right] d\eta \\
& \equiv \phi_d(\rho, z) + \phi_p(\rho, z)
\end{aligned} \tag{8}$$

The branches of the square roots in (8) are chosen so as to make their real parts positive for large values of ρ and z . It can be shown that this choice of branches for the square roots make their real parts positive for all values of ρ and z .

To obtain the desired integral representation for $\phi(\rho, z)$ we only have to make one more observation. The function $\phi_d(\rho, z)$ is the potential due to the charge density $\sigma_d(\rho)$ on the disk. This fact immediately implies that $\partial\phi_d/\partial z$ must vanish for $z=h$ and $\rho > a$, from which one can show that $g_d(\eta)$ has to be purely real, i.e.,

$$g_d^*(\eta) = g_d(\eta) \tag{9}$$

With (9) at hand we arrive at the following desired integral representation for $\phi(\rho, z)$:

$$\begin{aligned}
\phi(\rho, z) &= \frac{2V_0}{\pi} \int_0^b g_d(\eta) \operatorname{Re} \left\{ \frac{1}{\sqrt{(h+i\eta-z)^2 + \rho^2}} \right\} d\eta \\
&+ \frac{2V_0}{\pi} \int_a^\infty g_p(\eta) \operatorname{Im} \left\{ \frac{1}{\sqrt{(i\eta-z)^2 + \rho^2}} \right\} d\eta
\end{aligned} \tag{10}$$

2. FORMULATION OF AN INTEGRAL EQUATION

To formulate integral equations for $g_d(\eta)$ and $g_p(\eta)$ we invoke the boundary conditions on the disk and the ground plane, namely that

$$\phi(\rho, z) = V_0, \quad z = h, \quad 0 < \rho < b \quad (\text{disk}) \quad (11)$$

$$\phi(\rho, z) = 0, \quad z = 0, \quad a < \rho < \infty \quad (\text{ground plane})$$

The boundary conditions (11) imply that $g_d(\eta)$ and $g_p(\eta)$ must satisfy the following set of coupled integral equations:

$$\frac{\pi}{2} = \int_0^b g_d(\eta) \operatorname{Re} \left\{ \frac{1}{\sqrt{\rho^2 - \eta^2}} \right\} d\eta + \int_a^\infty g_p(\eta) \operatorname{Im} \left\{ \frac{1}{\sqrt{\rho^2 - (\eta + ih)^2}} \right\} d\eta, \quad 0 < \rho < b \quad (12)$$

$$0 = \int_0^b g_d(\eta) \operatorname{Re} \left\{ \frac{1}{\sqrt{\rho^2 - (\eta + ih)^2}} \right\} d\eta + \int_a^\infty g_p(\eta) \operatorname{Im} \left\{ \frac{1}{\sqrt{\rho^2 - \eta^2}} \right\} d\eta, \quad a < \rho < \infty$$

By changing ρ to $1/\rho$ in the second equation in (12) and η to $1/\eta$ in the second integral in both equations in (12) one obtains the following set of integral equations:

$$\frac{\pi}{2} = \int_0^\rho g_d(\eta) \frac{1}{\sqrt{\rho^2 - \eta^2}} d\eta + \int_0^{1/a} h_p(\eta) \operatorname{Im} \left\{ \frac{1}{\sqrt{\eta^2 \rho^2 - (1 + ih\eta)^2}} \right\} d\eta, \quad 0 < \rho < b \quad (13)$$

$$0 = \int_0^b g_d(\eta) \operatorname{Re} \left\{ \frac{1}{\sqrt{1 - \rho^2 (\eta + ih)^2}} \right\} d\eta + \int_0^\rho h_p(\eta) \frac{1}{\sqrt{\rho^2 - \eta^2}} d\eta, \quad 0 < \rho < 1/a$$

where

$$h_p(\eta) = g_p(1/\eta)/\eta$$

The set of integral equations (13) is of the first kind and thus not suitable for numerical solution. To obtain a set of Fredholm integral equations of the second kind which are amenable to numerical solution and for which an asymptotic solution can be found in some limiting cases we proceed as follows. First, we observe that the Abel integral equation

$$\int_0^{\rho} \frac{f_1(\eta)}{\sqrt{\rho^2 - \eta^2}} d\eta = f_2(\rho) \quad (14)$$

has the following solution (ref. 6)

$$f_1(\eta) = \frac{2}{\pi} \frac{d}{d\eta} \int_0^{\eta} \frac{\rho f_2(\rho)}{\sqrt{\eta^2 - \rho^2}} d\rho \quad (15)$$

Second, we consider momentarily $h_p(\eta)$ to be known in the first equation in (13) and $g_d(\eta)$ to be known in the second equation in (13). With the aid of the solution (15) of (14) we can then transform the set of integral equations (13) of the first kind into the following set of Fredholm integral equations of the second kind:

$$\begin{aligned} g_d(\eta) + \int_{\eta}^{1/a} K_1(\eta, \eta') h_p(\eta') d\eta' &= 1, \quad 0 < \eta < b \\ h_p(\eta) + \int_0^b K_2(\eta, \eta') g_d(\eta') d\eta' &= 0, \quad 0 < \eta < 1/a \end{aligned} \quad (16)$$

where

$$\begin{aligned} K_1(\eta, \eta') &= \frac{2}{\pi} \frac{d}{d\eta} \int_0^{\eta} \frac{\rho}{\sqrt{\eta^2 - \rho^2}} \operatorname{Im} \left\{ \frac{1}{\sqrt{\eta'^2 \rho^2 - (1 + i h \eta')^2}} \right\} d\rho \\ &= \frac{1}{\pi} \left\{ \frac{1 + \eta \eta'}{(1 + \eta \eta')^2 + h^2 \eta'^2} + \frac{1 - \eta \eta'}{(1 - \eta \eta')^2 + h^2 \eta'^2} \right\} \end{aligned}$$

and

$$\begin{aligned} K_2(\eta, \eta') &= \frac{2}{\pi} \frac{d}{d\eta} \int_0^{\eta} \frac{\rho}{\sqrt{\eta^2 - \rho^2}} \operatorname{Re} \left\{ \frac{1}{\sqrt{1 - \rho^2 (\eta' + i h)^2}} \right\} d\rho \\ &= \frac{1}{\pi} \left\{ \frac{1 + \eta \eta'}{(1 + \eta \eta')^2 + h^2 \eta'^2} + \frac{1 - \eta \eta'}{(1 - \eta \eta')^2 + h^2 \eta'^2} \right\} \end{aligned}$$

The set of coupled integral equations (16) can be reduced to one single integral equation for $g_d(\eta)$

$$g_d(\eta) - \int_0^b K(\eta, \eta') g_d(\eta') d\eta' = 1, \quad 0 < \eta < b \quad (17)$$

where

$$\begin{aligned} K(\eta, \eta') &= \int_0^{1/a} K_1(\eta, \eta'') K_2(\eta'', \eta') d\eta'' \\ &= \frac{1}{\pi^2} \left\{ \left[\frac{(\eta + \eta')^2 + 2h^2}{2(\eta + \eta')[(\eta + \eta')^2 + 4h^2]} - \frac{(\eta' - \eta)^2 + 2h^2}{2(\eta' - \eta)[(\eta' - \eta)^2 + 4h^2]} \right] \ln \left(\frac{(a + \eta)^2 + h^2}{(a - \eta)^2 + h^2} \right) \right. \\ &\quad + \left[\frac{(\eta + \eta')^2 + 2h^2}{2(\eta + \eta')[(\eta + \eta')^2 + 4h^2]} + \frac{(\eta' - \eta)^2 + 2h^2}{2(\eta' - \eta)[(\eta' - \eta)^2 + 4h^2]} \right] \ln \left(\frac{(a + \eta')^2 + h^2}{(a - \eta')^2 + h^2} \right) \\ &\quad + \left. \left[\frac{h}{(\eta - \eta')^2 + 4h^2} + \frac{h}{(\eta + \eta')^2 + 4h^2} \right] \left[\tan^{-1} \left(\frac{\eta^2 + h^2 + a\eta}{ah} \right) + \tan^{-1} \left(\frac{\eta^2 + h^2 - a\eta}{ah} \right) \right. \right. \\ &\quad \left. \left. + \tan^{-1} \left(\frac{\eta'^2 + h^2 + a\eta'}{ah} \right) + \tan^{-1} \left(\frac{\eta'^2 + h^2 - a\eta'}{ah} \right) \right] \right\} \end{aligned}$$

The function $h_p(\eta)$ is then readily obtained from the following integral expression:

$$h_p(\eta) = - \int_0^b K_2(\eta, \eta') g_d(\eta') d\eta' \quad 0 < \eta < 1/a \quad (18)$$

The two equations (17) and (18) are the desired integral equations for $g_d(\eta)$ and $h_p(\eta)$. In the general case it is not possible to find a closed-form solution of (17). One therefore has to resort to numerical means of "solving" (17). This will be done in section V. Before going on to do so we will, however, find asymptotic solutions of (17) for some limiting cases in section IV. In section III we will see how the solution of (17) can be used to find the capacitance between the disk and the ground plane. We will

also see in section III how the solutions of (17) and (18) can be used to find the dipole moment of the aperture and the effective height, equivalent area, and equivalent volume of the disk simulator.

SECTION III

CHARACTERISTIC QUANTITIES OF SIMULATOR

In this section we will see how the solution of (17) and (18) can be used to find the following characteristic quantities of the simulator:

(1) capacitance between the disk and the perforated ground plane, (2) the dipole moment of the aperture, and (3) the simulator's effective height, equivalent area, and equivalent volume.

1. CAPACITANCE BETWEEN DISK AND PERFORATED GROUND PLANE

To find the desired capacitance we only have to determine the total charge Q_d on the disk. The approach we use here to determine Q_d follows closely with that used by Love in reference 5. For that reason we observe from (8) that the potential $\phi_d(\rho, z)$ from the charges on the disk is given by

$$\phi_d(\rho, z) = \frac{V_0}{\pi} \int_{-b}^b \frac{g_d(\eta)}{\sqrt{(h+i\eta-z)^2 + \rho^2}} d\eta \quad (19)$$

For large values of $r = \sqrt{\rho^2 + z^2}$, one has

$$\phi_d(\rho, z) = \frac{Q_d}{4\pi\epsilon_0 r} + o(r^{-2}) \quad (20)$$

where Q_d is the total charge on the disk. Thus,

$$\begin{aligned} Q_d &= 4\epsilon_0 V_0 \lim_{r \rightarrow \infty} \left[r \int_{-b}^b \frac{g_d(\eta) d\eta}{\sqrt{r^2 + (h+i\eta)^2 - 2z(h+i\eta)}} \right] \\ &= 4\epsilon_0 V_0 \int_{-b}^b g_d(\eta) d\eta \\ &= 8\epsilon_0 V_0 \int_0^b g_d(\eta) d\eta \end{aligned} \quad (21)$$

From (21) it follows immediately that the capacitance C between the disk and the ground plane is given by

$$C = \frac{Q_d}{V_o} = 8\epsilon_o \int_0^b g_d(\eta) d\eta \quad (22)$$

Thus, once (17) is solved to yield $g_d(\eta)$ then the capacitance can be found from a simple integral of this solution.

2. DIPOLE MOMENT OF APERTURE

To calculate the dipole moment of the circular aperture, we first observe that it can be expressed in terms of the aperture potential $\phi(\rho, 0) = \phi_d(\rho, 0) + \phi_p(\rho, 0)$ in the following way (ref. 7):

$$\begin{aligned} p &= \epsilon_o \int \phi(\rho, 0) dS \\ &= 2\pi\epsilon_o \int_0^a \rho \phi(\rho, 0) d\rho \end{aligned} \quad (23)$$

Inserting the expression (8) for $\phi(\rho, 0)$ into (23) results in the following expression:

$$\begin{aligned} p &= 4\epsilon_o V_o \int_0^a \rho d\rho \int_0^b g_d(\eta) \operatorname{Re} \left\{ \frac{1}{\sqrt{\rho^2 + (h + i\eta)^2}} \right\} d\eta \\ &\quad + 4\epsilon_o V_o \int_0^a \rho d\rho \int_a^\infty g_p(\eta) \frac{1}{\sqrt{\eta^2 - \rho^2}} d\eta \\ &= 4\epsilon_o V_o \int_0^b \left[\operatorname{Re} \left\{ \sqrt{a^2 + (h + i\eta)^2} \right\} - h \right] g_d(\eta) d\eta \\ &\quad + 4\epsilon_o V_o \int_a^\infty \left[\eta - \sqrt{\eta^2 - a^2} \right] g_p(\eta) d\eta \end{aligned}$$

$$\begin{aligned}
&= 4\epsilon_0 V_0 \int_0^b \left[\operatorname{Re} \left\{ \sqrt{a^2 + (h + i\eta)^2} \right\} - h \right] g_d(\eta) d\eta \\
&+ 4\epsilon_0 V_0 \int_0^{1/a} \left[1 - \sqrt{1 - \eta^2 a^2} \right] h_p(\eta) / \eta^2 d\eta
\end{aligned} \tag{24}$$

Therefore, the dipole moment can be calculated from (24) once $g_d(\eta)$ and $h_p(\eta)$ are determined from (17) and (18).

3. SIMULATOR'S EFFECTIVE HEIGHT

The effective height of the simulator is defined from the problem depicted in figure 4a, where a uniform static field E_0 is applied to the disk-ground-plane configuration. With the total charge on the disk being zero and its potential being V_1 the effective height h_{eff} is defined from the relationship

$$V_1 = h_{\text{eff}} E_0 \tag{25}$$

Although h_{eff} is defined from a different problem than the one that yields C and p we will now see how the Lorentz reciprocity theorem can be used to relate h_{eff} , r and C .

Consider first the problem of figure 4a. The potential $\phi_1(\rho, z)$ must satisfy the following conditions:

$$\nabla^2 \phi_1 = 0 \quad \text{off disk and ground plane} \tag{26}$$

$$\phi_1(\rho, z) = \begin{cases} 0, & \text{on } S_p \text{ (ground plane)} \\ V_1, & \text{on } S_d \text{ (disk)} \\ E_0 z = E_0 r \cos \theta, & \text{on } S_\infty^+ (r = \sqrt{\rho^2 + z^2} \rightarrow \infty, z > 0) \\ 0(r^{-2}), & \text{on } S_\infty^- (r = \sqrt{\rho^2 + z^2} \rightarrow \infty, z < 0) \end{cases} \tag{27}$$

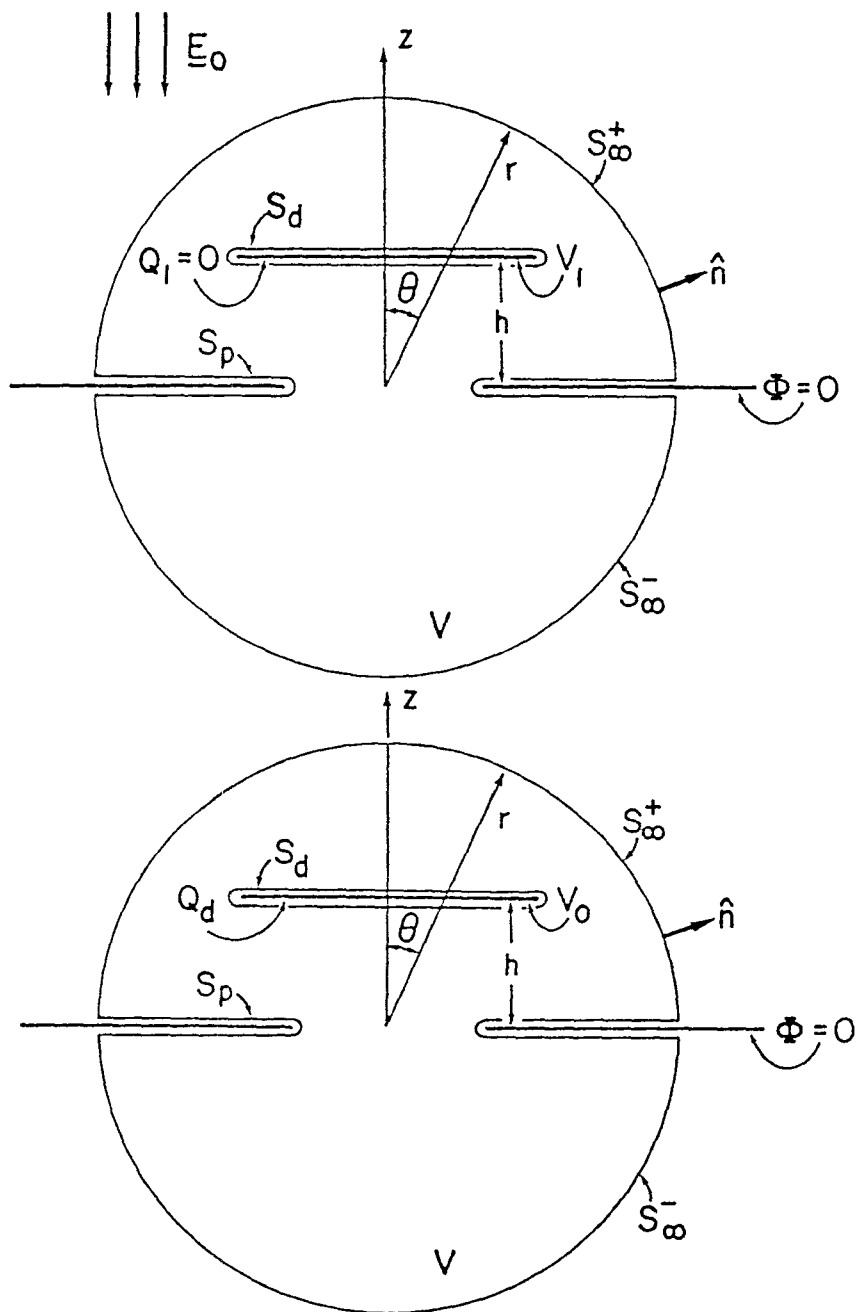


Figure 4. The Receiving Problem (a) and the Capacitance Problem (b) Used in the Lorentz Reciprocity Theorem.

Next, consider the problem of figure 4b. This is the problem considered in section II. It is easy to see that the potential $\phi(\rho, z)$ of this problem satisfies the following conditions:

$$\nabla^2 \phi = 0 \quad \text{off disk and ground plane} \quad (28)$$

$$\phi(\rho, z) = \begin{cases} 0, & \text{on } S_p \\ V_0, & \text{on } S_d \\ \frac{(hQ_d + p) \cos \theta}{2\pi\epsilon_0 r^2}, & \text{on } S_\infty^+ \\ \frac{p \cos \theta}{2\pi\epsilon_0 r^2}, & \text{on } S_\infty^- \end{cases} \quad (29)$$

We now apply the Lorentz reciprocity theorem to the region V bounded by S_d , S_p , and S_∞^\pm . This results in the following expression:

$$\begin{aligned} 0 &= \int_V (\phi \nabla^2 \phi_1 - \phi_1 \nabla^2 \phi) dV \\ &= \int_{S_p + S_d + S_\infty^+ + S_\infty^-} (\phi \nabla \phi_1 - \phi_1 \nabla \phi) \cdot \hat{n} dS \\ &= -\frac{V_1 Q_d}{\epsilon_0} + \int_{S_\infty^+} (\phi \nabla \phi_1 - \phi_1 \nabla \phi) \cdot \hat{n} dS \\ &= -\frac{V_1 Q_d}{\epsilon_0} + 2\pi \int_0^{\pi/2} \frac{3E_0}{2\pi\epsilon_0} (Q_d h + p) \cos^2 \theta \sin \theta d\theta \\ &= -\frac{V_1 Q_d}{\epsilon_0} + \frac{(Q_d h + p)}{\epsilon_0} E_0 \end{aligned} \quad (30)$$

where \hat{n} is the unit outward normal vector of the surface $S_p + S_d + S_\infty^+ + S_\infty^-$. Furthermore, we have used the fact that the discontinuity of $\nabla\phi$ across S_d is equal to $\epsilon_0^{-1}\sigma_d$. Thus, (30) results in the following expression for the effective height:

$$h_{\text{eff}} = \frac{V_1}{E_0} = h + \frac{P}{Q_d} = h + \frac{P}{CV_0} \quad (31)$$

4. SIMULATOR'S EQUIVALENT AREA AND VOLUME

The equivalent area of the simulator is determined from the problem of figure 5. In this problem, the disk and the ground plane are held at the same potential (disk short circuited to ground plane). The equivalent area A_{eq} is defined through the relationship (ref. 8):

$$Q_2 = A_{\text{eq}} \epsilon_0 E_0 \quad (32)$$

To relate A_{eq} to the other characteristic quantities of the simulator we use antenna theory. Define a port A,B where A is a point on the disk and B is a point on the ground plane (figure 5). We then have the Thévenin and Norton equivalent circuits of figure 6. In these circuits the parameters are defined by

$$\begin{aligned} Y_{\text{in}} &= j\omega C \\ V_{\text{oc}} &= h_{\text{eff}} E_0 \\ I_{\text{sc}} &= j\omega Q_2 = j\omega A_{\text{eq}} \epsilon_0 E_0 \end{aligned} \quad (33)$$

But it is also well-known that

$$I_{\text{sc}} = Y_{\text{in}} V_{\text{oc}} \quad (34)$$

from which it follows that

$$A_{\text{eq}} = h_{\text{eff}} C / \epsilon_0 \quad (35)$$

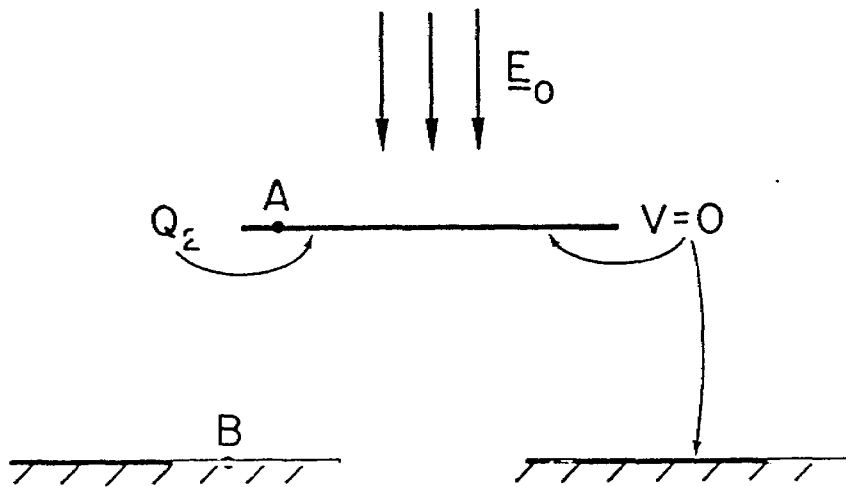


figure 5

Figure 5. The Simulator Problem Defining the Equivalent Area.

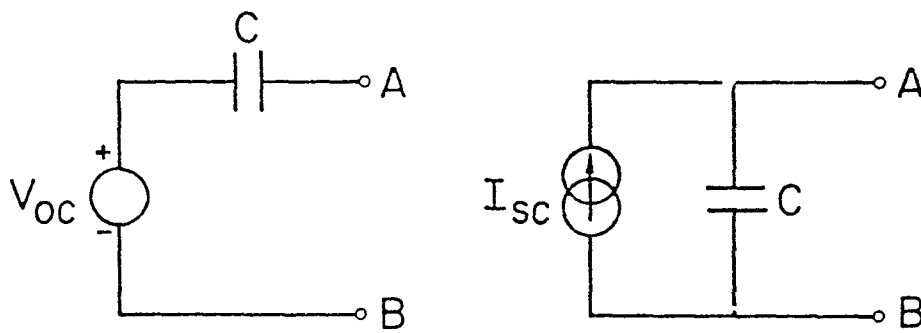


figure 6

Figure 6. The Low Frequency Thévenin and Norton Equivalent Circuits of the Simulator.

The equivalent volume V_{eq} is given by (ref. 8):

$$V_{eq} = h_{eff} A_{eq} = h_{eff}^2 C / \epsilon_0 \quad (36)$$

SECTION IV
SOME LIMITING CASES

In this section we will find asymptotic solutions of (17) and (18) in some limiting cases. These solutions will then be used to find asymptotic expressions for C , p , h_{eff} , A_{eq} , and V_{eq} in certain limiting cases.

1. THE CASE $h \gg a$, $h \gg b$

In this case, the interaction between the disk and the ground plane is weak. Consequently the solution for $g_d(\eta)$ is very close to the case of a disk in free space. An asymptotic solution of (17) and (18) results in the following expressions:

$$g_d(\eta) = 1 + b/(\pi h) + O(b^2/h^2) + O(a^2/h^2) + O(ab/h^2) \quad (37)$$

$$h_p(\eta) = -\frac{2}{\pi} \frac{b}{1+h^2\eta^2} \left(1 + \frac{b}{\pi h}\right) + O(b^2/h^2) + O(a^2/h^2) + O(ab/h^2)$$

The solution to the problem of a disk in free space is given by $g_d(\eta) = 1$.

From (22), (24), (31), (35), (36) and (37), one obtains the following asymptotic representations:

$$C \approx 8\epsilon_0 b [1 + b/(\pi h)]$$

$$p \approx \frac{8\epsilon_0 V_0}{3\pi} \frac{a^3 b}{h^2} \left(1 + \frac{b}{\pi h}\right)$$

$$V_{\text{eq}} \approx 8bh^2 \left(1 + \frac{b}{\pi h} + \frac{2a^3}{3\pi h^3}\right)$$

$$h_{\text{eff}} \approx h \left(1 + \frac{a^3}{3\pi h^3}\right)$$

$$A_{\text{eq}} \approx 8bh \left(1 + \frac{b}{\pi h} + \frac{a^3}{3\pi h^3}\right) \quad (38)$$

2. THE CASE $b \ll a$

In this case, the kernels $K_1(\eta, \eta')$ and $K_2(\eta, \eta')$ in the set of integral equations (16) can be approximated by the following expressions:

$$K_1(\eta, \eta') \approx \frac{2}{\pi} \frac{1}{1+h^2 \eta'^2}, \quad \text{for } 0 < \eta < b, \quad 0 < \eta' < 1/a \quad (39)$$

$$K_2(\eta, \eta') \approx \frac{2}{\pi} \frac{1}{1+h^2 \eta^2}, \quad \text{for } 0 < \eta < 1/a, \quad 0 < \eta' < b$$

With these simplified expressions the following closed-form solution of (16) is found:

$$g_d(\eta) \approx \left[1 - \frac{2b}{\pi^2 h} \left(\tan^{-1}\left(\frac{h}{a}\right) + \frac{ah}{a^2+h^2} \right) \right]^{-1} \quad (40)$$

$$h_p(\eta) \approx -\frac{2}{\pi} \frac{b}{1+h^2 \eta^2} g_d(\eta)$$

The solution (40) results in the following expressions for C , p , and h_{eff} :

$$C \approx 8\epsilon_0 b \left[1 - \frac{2b}{\pi^2 h} \left(\tan^{-1}\left(\frac{h}{a}\right) + \frac{ah}{a^2+h^2} \right) \right]^{-1}$$

$$p \approx 4\epsilon_0 b V_0 \left[1 - \frac{2b}{\pi^2 h} \left(\tan^{-1}\left(\frac{h}{a}\right) + \frac{ah}{a^2+h^2} \right) \right]^{-1} \quad (41)$$

$$\times \left\{ (\sqrt{a^2+h^2} - h) + \frac{2a}{\pi} \left[1 - \frac{\pi}{2} \left(1 + \frac{h^2}{a^2} \right)^{\frac{1}{2}} + \frac{h}{a} \tan^{-1} \frac{h}{a} \right] \right\}$$

$$h_{\text{eff}} = h + \frac{1}{2} \left\{ (\sqrt{a^2+h^2} - h) + \frac{2a}{\pi} \left[1 - \frac{\pi}{2} \left(1 + \frac{h^2}{a^2} \right)^{\frac{1}{2}} + \frac{h}{a} \tan^{-1} \frac{h}{a} \right] \right\}$$

We observe that the above results for C , p and h_{eff} reduce to those of Case 1 when $h \gg a$. Furthermore, the expressions for C and $A_{\text{eq}} = h_{\text{eff}} C / \epsilon_0$ reduce to those presented in reference 9 for the case where $h = 0$.

3. THE CASE $a = 0$

By putting $a = 0$ in (17), one obtains the following integral equation for $g_d(\eta)$:

$$g_d(\eta) - \frac{2h}{\pi} \int_{-b}^b \frac{g_d(\eta') d\eta'}{(\eta - \eta')^2 + 4h^2} = 1 \quad (42)$$

This is the same equation as that derived in reference 4 for two coaxial disks of equal but opposite charge (or, equivalently, one charged disk above a ground plane). This equation has been studied extensively in references 4 and 5.

4. THE CASE $h = 0$, $a < D$

In this case, the kernels $K(\eta, \eta')$ and $K_2(\eta, \eta')$ in (17) and (18) reduce to the following expressions:

$$K(\eta, \eta') = \frac{2}{\pi^2} \left\{ \eta' \ln \left(\frac{a + \eta'}{a - \eta'} \right) - \eta \ln \left(\frac{a + \eta}{a - \eta} \right) \right\} \frac{1}{\eta'^2 - \eta^2} \quad (43)$$

$$K_2(\eta, \eta') = \frac{2}{\pi} \frac{1}{1 - \eta^2 \eta'^2}$$

These kernels are still too complicated to allow us to obtain analytic solutions for $g_d(\eta)$ and $h_p(\eta')$. However, this case has been treated in reference 9, and so it serves as a useful case for checking the results of the numerical solution.

SECTION V
NUMERICAL CALCULATIONS

In this section we will first "solve" (17) and (18) numerically. The numerical solutions of $g_d(\eta)$ and $h_p(\eta)$ will then be used to find C , p , h_{eff} , A_{eq} , and V_{eq} .

1. APPROXIMATION OF (17) BY A MATRIX EQUATION

The integral equation (17) can not be solved analytically for arbitrary values of a , b , and h . One therefore has to use numerical means of "solving" the equation. Since the kernel $K(\eta, \eta')$ is well behaved the numerical procedures we use are straightforward. The trapezoidal rule of evaluating the integral (17) leads us to the following matrix equation:

$$g_d(\eta_i) - \frac{b}{N} \sum_{j=0}^N \alpha_j K(\eta_i, \eta_j) g_d(\eta_j) = 1, \quad i = 0, 1, 2, \dots, N$$

where

$$\alpha_j = \begin{cases} 1/2, & j = 0, N \\ 1, & \text{otherwise} \end{cases} \quad (44)$$

$$\eta_i = ib/N$$

$$K(\eta_i, \eta_j) = \frac{1}{\pi^2} \left\{ \frac{(\eta_i + \eta_j)^2 + 2h^2}{2(\eta_i + \eta_j)[(\eta_i + \eta_j)^2 + 4h^2]} \ln \left(\frac{[(a + \eta_i)^2 + h^2][(a + \eta_j)^2 + h^2]}{[(a - \eta_i)^2 + h^2][(a - \eta_j)^2 + h^2]} \right) \right. \\ \left. + \frac{(\eta_j - \eta_i)^2 + 2h^2}{2(\eta_j - \eta_i)[(\eta_j - \eta_i)^2 + 4h^2]} \ln \left(\frac{[(a + \eta_j)^2 + h^2][(a - \eta_i)^2 + h^2]}{[(a - \eta_j)^2 + h^2][(a + \eta_i)^2 + h^2]} \right) \right\}$$

$$\begin{aligned}
& + \left[\frac{h}{(\eta_j - \eta_i)^2 + 4h^2} + \frac{h}{(\eta_j + \eta_i)^2 + 4h^2} \right] \times \left[\tan^{-1} \left(\frac{\eta_i^2 + h^2 + a\eta_i}{ah} \right) \right. \\
& \left. + \tan^{-1} \left(\frac{\eta_i^2 + h^2 - a\eta_i}{ah} \right) + \tan^{-1} \left(\frac{\eta_j^2 + h^2 + a\eta_j}{ah} \right) + \tan^{-1} \left(\frac{\eta_j^2 + h^2 - a\eta_j}{ah} \right) \right] \Bigg\} \\
& \text{for } \eta_i \neq \eta_j
\end{aligned}$$

and

$$\begin{aligned}
K(\eta_i, \eta_i) &= \frac{1}{2\pi^2} \left\{ \left[\frac{a - \eta_i}{(a - \eta_i)^2 + h^2} + \frac{a + \eta_i}{(a + \eta_i)^2 + h^2} \right] \right. \\
& + \left(\frac{h}{\eta_i^2 + h^2} + \frac{1}{h} \right) \left[\tan^{-1} \left(\frac{\eta_i^2 + h^2 + a\eta_i}{ah} \right) + \tan^{-1} \left(\frac{\eta_i^2 + h^2 - a\eta_i}{ah} \right) \right] \\
& \left. + \frac{2\eta_i^2 + h^2}{2\eta_i(\eta_i^2 + h^2)} \ln \left[\frac{(a + \eta_i)^2 + h^2}{(a - \eta_i)^2 + h^2} \right] \right\} .
\end{aligned}$$

Once the function values $g_d(\eta_i)$ have been found, the quantities $h_p(\eta_j)$.
C, p are simply given by the following expressions:

$$\begin{aligned}
h_p(\eta_j) &= -\frac{b}{N} \sum_{i=0}^N \alpha_i K_2(\eta_j, \eta_i) g_d(\eta_i), \quad j=0, 1, 2, \dots, M \\
C &= 8\epsilon_0 \frac{b}{N} \sum_{i=0}^N \alpha_i g_d(\eta_i) \\
p &= 4\epsilon_0 V_0 \frac{b}{N} \sum_{j=0}^N \alpha_j \left[\operatorname{Re} \left\{ \sqrt{a^2 + (h + i\eta_j)^2} \right\} - h \right] g_d(\eta_j) \\
&+ 4\epsilon_0 V_0 \frac{1}{aM} \sum_{j=0}^M \alpha_j \left[1 - \sqrt{1 - \eta_j'^2 a^2} \right] h_p(\eta_j') / \eta_j'^2
\end{aligned} \tag{45}$$

where

$$\eta_j' = j \frac{1}{aM}$$

$$K_2(\eta_j', \eta_i) = \frac{1}{\pi} \left\{ \frac{1 + \eta_j' \eta_i}{(1 + \eta_j' \eta_i)^2 + h^2 \eta_j'^2} + \frac{1 - \eta_j' \eta_i}{(1 - \eta_j' \eta_i)^2 + h^2 \eta_j'^2} \right\}$$

2. ACCURACY OF NUMERICAL SOLUTION

Equations (44) and (45) contain the two integers M and N . The integer N determines the size of the matrix in (44) and thus the accuracy with which we determine $g_d(\eta)$. To determine this accuracy we solve (44) for two different values of N , namely $N=N_1$ and $N=2N_1$. For each of these cases we calculate the norm of $g_d(\eta)$, defined by

$$\|g_d\|_N = \frac{1}{N+1} \sum_{j=0}^N |g_d(\eta_j)|^2 \quad (46)$$

The value of N_1 is then determined such that

$$\left| \|g_d\|_{2N_1} - \|g_d\|_{N_1} \right| < \epsilon \|g_d\|_{N_1} \quad (47)$$

It was found that $2N_1=64$ always result in $\epsilon < 5 \times 10^{-3}$ (except when h/a and a/b are both very small). We considered this accuracy sufficient for our purposes and so (44) was solved using the value $N=64$. Similarly, it was found that $M=64$ results in sufficiently accurate values for $h_p(\eta)$.

To gain some more confidence in the numerical solution we consider the special case where $h=0$ and $a > b$. This case has been treated in detail in reference 9. In table 1 we compare the capacitance and equivalent area as obtained from the numerical calculations of this report and those of reference 9. We consider the agreement very good.

Table 1

COMPARISONS OF THE CAPACITANCE AND EQUIVALENT AREA
BETWEEN THE PRESENT RESULTS AND THOSE OF LATHAM AND LEE GIVEN IN REFERENCE 5

b/a	$C/(\beta\epsilon_0 b)$		$A_{eq}/(\pi ab)$	
	Latham and Lee	Present Results	Latham and Lee	Present Results
0.1	1.04234	1.04234	0.842066	0.841611
0.2	1.08908	1.08908	0.870903	0.870418
0.3	1.14172	1.14172	0.897127	0.896602
0.4	1.20244	1.20244	0.920746	0.920162
0.5	1.27463	1.27465	0.941726	0.941070
0.6	1.36404	1.36407	0.959985	0.959222
0.7	1.48155	1.48164	0.975367	0.974438
0.8	1.65203	1.65231	0.987607	0.986375
0.9	1.95649	1.95800	0.996221	0.995240

3. NUMERICAL RESULTS FOR C , p , h_{eff} , A_{eq} , AND V_{eq}

The results of the numerical calculations are shown in figures 7 through 12. All results for C , h_{eff} , A_{eq} , and V_{eq} presented in figures 8, 10, 11, and 12 have been normalized with respect to the values of the corresponding quantity in the case where the aperture is absent ($a=0$). Figure 7 shows the variation of C with h/b when $a=0$. In this graph we have normalized C with respect to (i) the capacitance of one disk in free space, $8\epsilon_0 b$, and (ii) the limiting value of the capacitance between a disk and a ground plane when $h \ll b$, this value being $\epsilon_0 \pi b^2/h$. The broken lines in figure 7 correspond to the asymptotic results (38). Furthermore, $h_{eff} = h$ and $p = 0$ in the case where $a=0$. Thus, $A_{eq} = hC/\epsilon_0$ and $V_{eq} = h_{eff} A_{eq} = h^2 C/\epsilon_0$ when $a=0$ and so both A_{eq} and V_{eq} are proportional to C in this case.

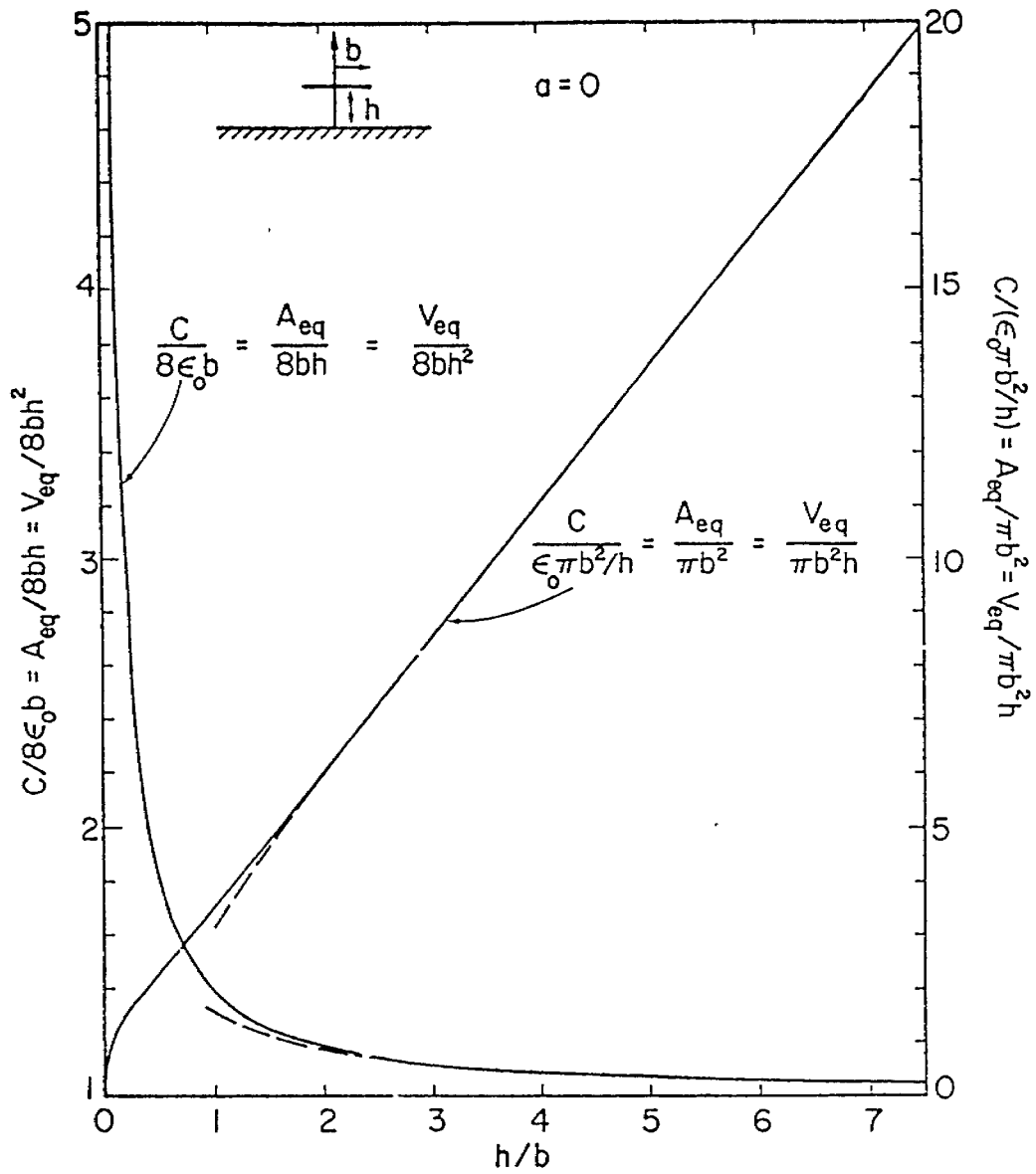


Figure 7. Capacitance, Equivalent Area, and Equivalent Volume of a Circular Disk Above a Ground Plane. The Broken Curves Correspond to the Asymptotic Results of Equation (38).

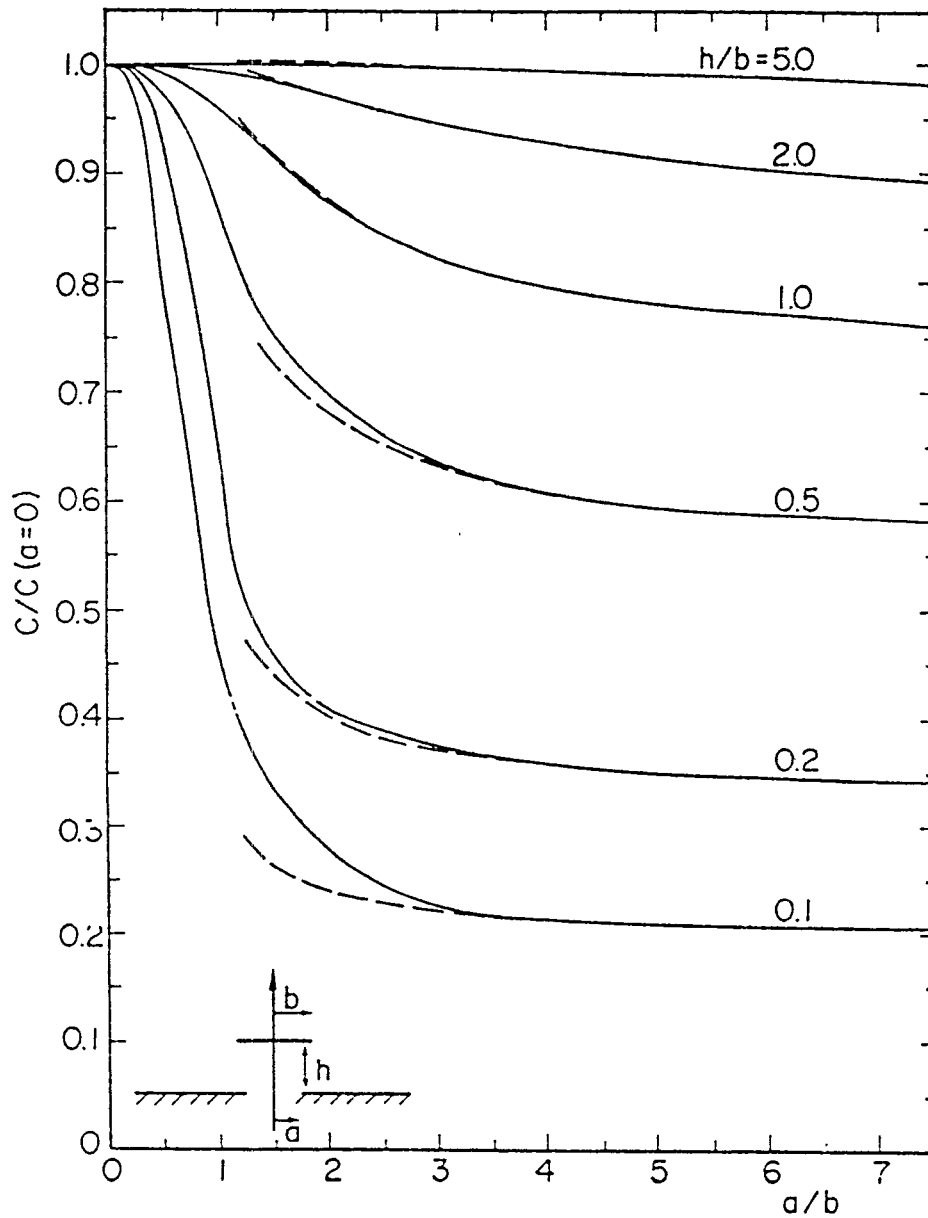


Figure 8. Variation of Simulator Capacitance with Position of Disk and Size of Aperture. The Values are Normalized with Respect to the Capacitance in the Absence of the Aperture. The Broken Curves Correspond to the Asymptotic Results of Equation (38).

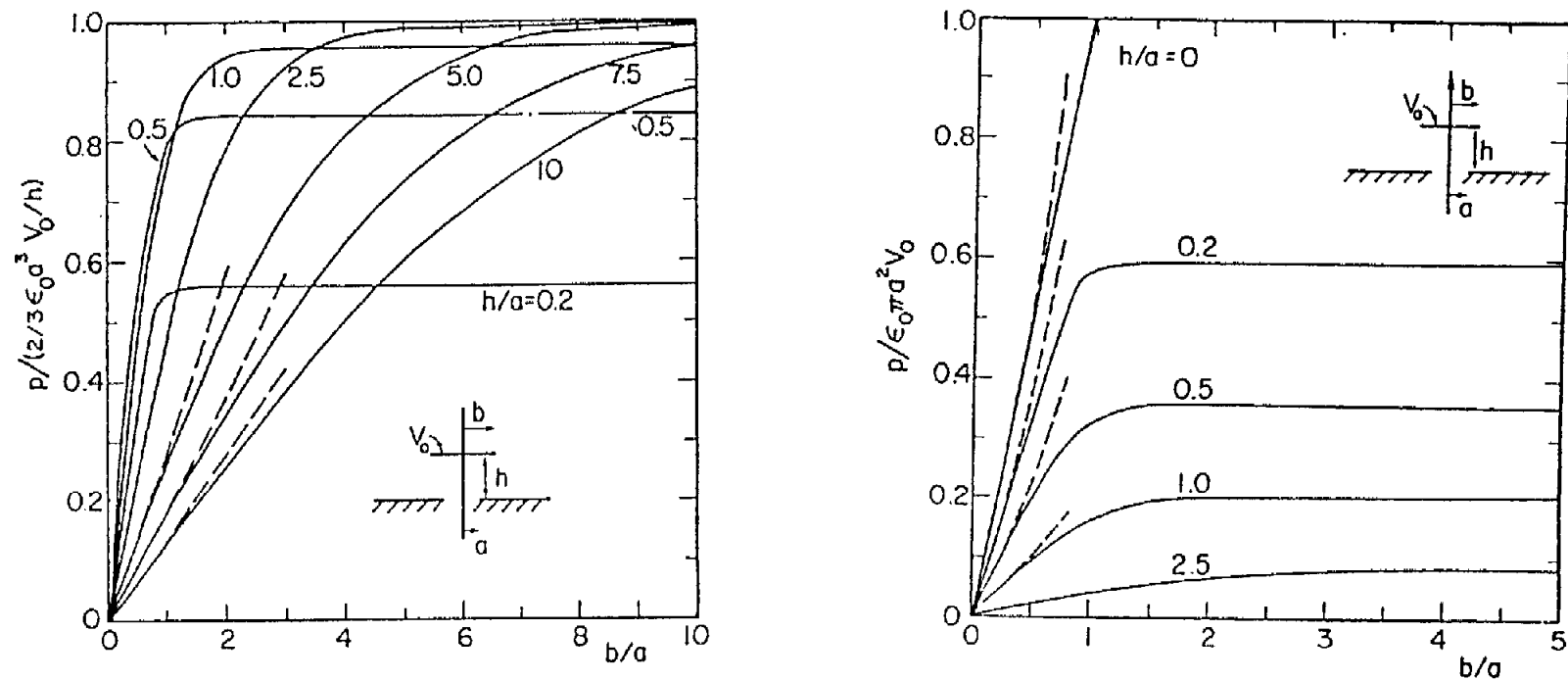


Figure 9. Variation of the Aperture Dipole Moment with Position and Size of Simulator Disk.

- (a) The Values are Normalized with Respect to the Dipole Moment of the Aperture when Subject to a Uniform, Normal Electric Field Strength V_0/h .
- (b) The Values are Normalized with Respect to the Limiting Value of the Dipole Moment as $h/a \ll 1$ and $b/a \gg 1$.

The Broken Curves Correspond to the Asymptotic Results of Equation (41).

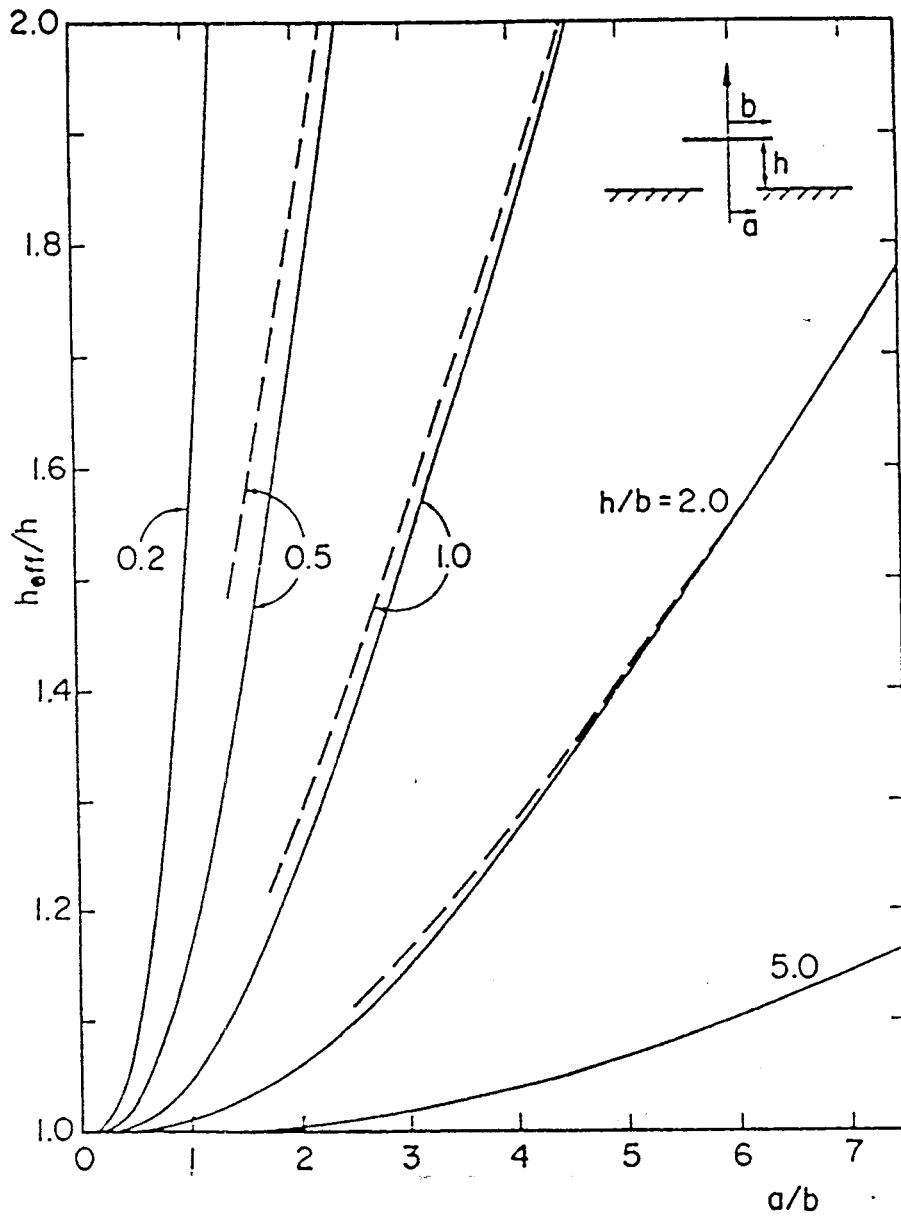


Figure 10. Variation of Simulator Effective Height with Position of Disk and Size of Aperture. The Broken Curves Correspond to the Asymptotic Results of Equation (41).

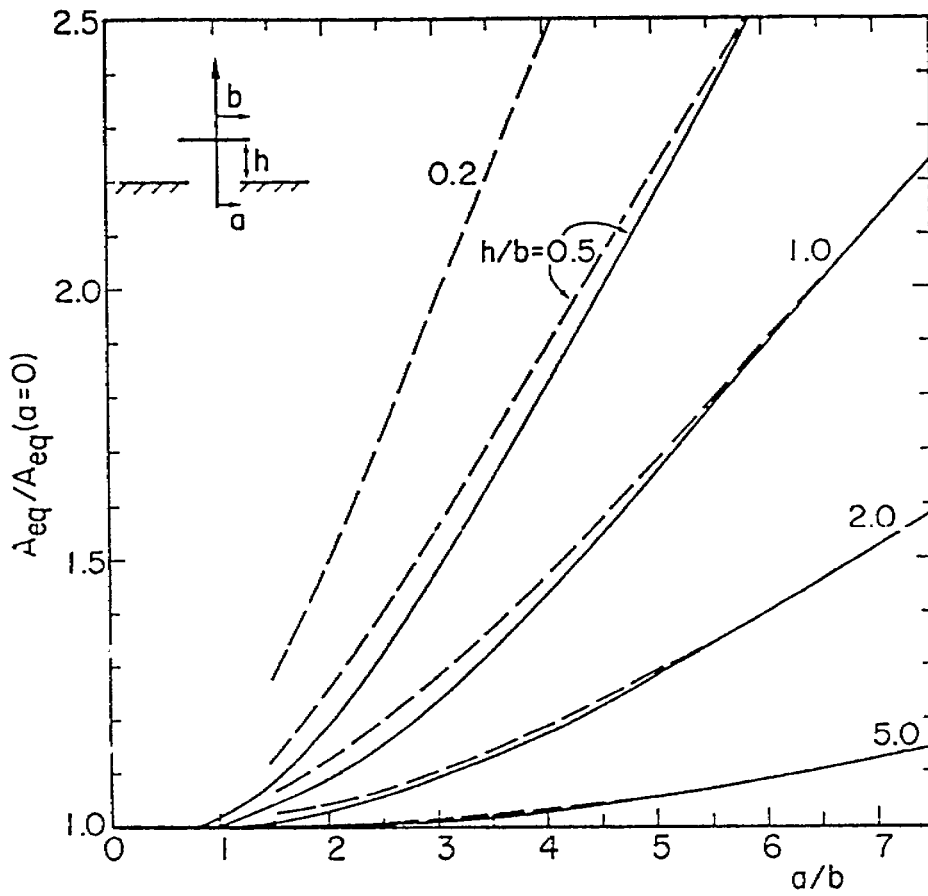


Figure 11. Variation of Simulator Equivalent Area with Position of Disk and Size of Aperture. The Values are Normalized with Respect to the Equivalent Area in the Absence of the Aperture. The Broken Curves Correspond to the Asymptotic Results of Equation (41).

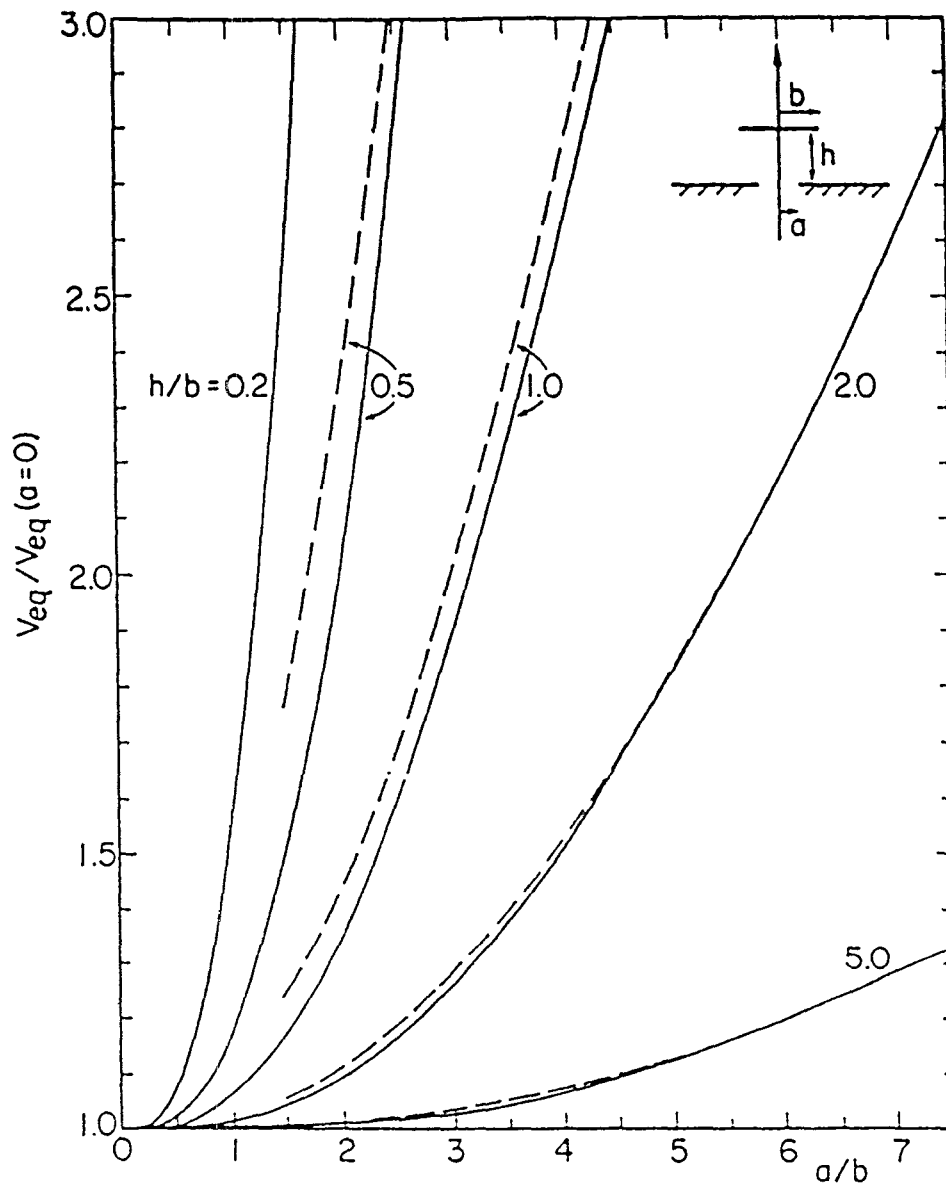


Figure 12. Variation of Simulator Equivalent Volume with Position of Disk and Size of Aperture. The Values are Normalized with Respect to the Equivalent Volume in the Absence of the Aperture. The Broken Curves Correspond to the Asymptotic Results of Equation (41).

The variation of the capacitance between the disk and the ground plane as the hole size varies is shown in figure 8 for various separations between the disk and the ground plane. The broken curves in figure 8 correspond to the asymptotic results (41).

Figures 9a and 9b display the variation of the aperture dipole moment p with respect to b/a and h/a . In figure 9a we have normalized p with respect to $(2\epsilon_0 a^3/3)(V_0/h)$ which is the dipole moment of a circular hole in an infinite ground plane subject to a uniform, normal electric field of strength V_0/h . The results of figure 9a show that for fixed values of V_0/h then the interaction between the simulator and the test object decreases the excitation of the aperture. These results also show that the interaction only decreases the dipole moment with approximately 5% when $h/a = 1$ and $b/a > 2$. The simulator-aperture interaction is stronger for $h/a < 1$ thus decreasing the dipole moment even further. Figure 9b shows the dipole moment normalized with respect to $\epsilon_0 \pi a^2 V_0$.

The effective height h_{eff} normalized with respect to h is shown in figure 10. The broken curves represent the asymptotic results (41). We observe from figure 10 that the results (41) are valid within 10% for $h/b > 0.5$ and $a/b > 1.5$.

The simulator's equivalent area and volume are graphed in figures 11 and 12 versus a/b for various values of h/b . The broken curves represent the asymptotic results (41).

REFERENCES

- [1] Baum, C.E., "EMP Simulators for Various Types of Nuclear EMP Environments: An Interim Categorization," Sensor and Simulation Note 151, July 1972. Also Appears in Special EMP Issue of Trans. Antennas Propagat. and Electromagnetic Compatibility, January 1978.
- [2] Chen, L.W. and C.E. Baum, "Performance Parameters Associated with the FINES-Type Small EMP Simulators," Sensor and Simulation Note, to be published.
- [3] Whittaker, E.T. and G.N. Watson, A Course of Modern Analysis, American ed., Cambridge University Press, 1948, Chapter 18.
- [4] Lam, John, "Potential of a Charge Cylinder," Caltech Antenna Lab. Tech. Report No. 41, August 1967.
- [5] Love, E.R., "The Electrostatic Field of Two Equal Circular Coaxial Conducting Disks," Quart. J. Mech. and Appl. Math., Vol. 2, 1948, p.428.
- [6] Sneddon, I.N., Mixed Boundary Value Problems in Potential Theory, North-Holland Publishing Company, 1966, p.41.
- [7] Lee, K.S.H. and C.E. Baum, "Application of Model Analysis to Braided-Shield-Cables," Interaction Note 132, November 1973. Also appears in IEEE Trans. Electromagnetic Compatibility, Vol. EMC-17, August 1975.
- [8] Baum, C.E., "Parameters for Some Electrically-Small Electromagnetic Sensors," Sensor and Simulation Note 38, March 1967.
- [9] Latham, R.W. and K.S.H. Lee, "Capacitance and Equivalent Area of a Disk in a Circular Aperture," Sensor and Simulation Note 106, May 1970.
- [10] Baum, C.E., "Some Types of Small EMP Simulators," Miscellaneous Simulator Memo 9, December 1976.